

Differentiable Artificial Reverberation

Sungho Lee, Hyeong-Seok Choi, and Kyogu Lee

Abstract—Artificial reverberation (AR) models play a central role in various audio applications. Therefore, estimating the AR model parameters (ARPs) of a target reverberation is a crucial task. Although a few recent deep-learning-based approaches have shown promising performance, their non-end-to-end training scheme prevents them from fully exploiting the potential of deep neural networks. This motivates the introduction of differentiable artificial reverberation (DAR) models, allowing loss gradients to be back-propagated end-to-end. However, implementing the AR models with their difference equations “as is” in the deep-learning framework severely bottlenecks the training speed when executed with a parallel processor like GPU due to their infinite impulse response (IIR) components. We tackle this problem by replacing the IIR filters with finite impulse response (FIR) approximations with the frequency-sampling method (FSM). Using the FSM, we implement three DAR models—differentiable Filtered Velvet Noise (FVN), Advanced Filtered Velvet Noise (AFVN), and Feedback Delay Network (FDN). For each AR model, we train its ARP estimation networks for analysis-synthesis (RIR-to-ARP) and blind estimation (reverberant-speech-to-ARP) task in an end-to-end manner with its DAR model counterpart. Experiment results show that the proposed method achieves consistent performance improvement over the non-end-to-end approaches in both objective metrics and subjective listening test results. Audio samples are available at <https://sh-lee97.github.io/DAR-samples/>.

Index Terms—Digital Signal Processing, Acoustics, Reverberation, Artificial Reverberation, Deep Learning.

I. INTRODUCTION

Reverberation is ubiquitous in a real acoustic environment. It provides the listeners psychoacoustic cues for spatial presence. Therefore, adding an appropriate reverberation to a dry audio is crucial for plausible listening [1]–[3]. *Artificial reverberation* (AR), efficient digital filters that mimic real-world reverberation, have been developed to achieve such auditory effects [4]–[6] and applied to room acoustic enhancement [7], auditory scene generation [8], [9], post-production [10], and many more.

Nevertheless, estimating the AR model parameters (ARPs) that match the target reverberation remains challenging. This is because the mapping from the ARPs to the reverberation is highly nontrivial. We refer to this task as *analysis-synthesis* and *blind estimation* when the target is a room impulse response (RIR) and reverberant speech, respectively.

ARP estimation is a classical problem, and various attempts have been made [11]–[14]. However, they are only applicable to a specific AR model (AR-model-dependent) and the analysis-synthesis task (task-dependent). This inflexibility is problematic since every application has its own suitable AR models and target forms (e.g., RIR and reverberant speech).

Manuscript submitted to TASLP. The authors are with the Music and Audio Research Group (MARG), Seoul National University, Seoul, Republic of Korea (e-mail: sh-lee@snu.ac.kr; kekepa15@snu.ac.kr; kglee@snu.ac.kr).

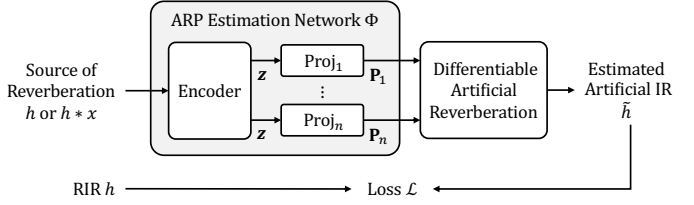


Fig. 1. The proposed ARP estimation framework. With the DAR models, loss gradients $\partial \mathcal{L} / \partial \mathbf{P}_1, \dots, \partial \mathcal{L} / \partial \mathbf{P}_n$ can be back-propagated through the DAR models. Hence, the ARP estimation network Φ can be trained in an end-to-end manner. We can train the network to perform the analysis-synthesis (RIR h input), blind estimation (reverberant speech $h * x$ input), or even both. The network has an AR-model-agnostic encoder so that using a different DAR model only requires changing the tiny projection layers $\text{Proj}_1, \dots, \text{Proj}_n$.

Despite being proposed for a single task and AR model, recent data-driven approaches [10], [15] showed promises of mitigating such dependencies. That is, a deep neural network (DNN) can be applied to any AR model and task. However, when the training objectives are defined on the ARP domain, and their performance could be suboptimal for two reasons. First, the ARP domain distance hardly matches the perceptual one. For example, multiple ARP sets can result in the same IR, i.e., many-to-one. Second, the AR model itself must generate the target reverberation to obtain the ground-truth ARP, which is cumbersome and increases the generalization error.

One could overcome these limitations with *differentiable artificial reverberation* (DAR) models. With the DAR models, a loss between the target IR and the estimation can be calculated and back-propagated to train the DNNs without any explicit ARP evaluation (see Figure 1). In this framework, we can use perceptually relevant objectives instead of the ARP-matching ones, which improve the performance. Also, we can use any unlabeled RIR data to train the network.

Since the AR models are exactly or close to linear time-invariant (LTI) systems, we can implement them differentiably “as is” with their difference equations [16]–[19]. However, this approach has been impractical since their infinite impulse response (IIR) filter components bottleneck the training speed when executed in a parallel processor, e.g., GPU. Alternatively, one can model reverberation with DNNs instead of using the AR models [20]–[24]. While these approaches achieve high-quality reverberation, the AR models still could be favored for the multiple reasons. First, they are more directly interpretable and controllable, allowing end-users (e.g., audio engineers) to further tune the parameters. Second, their structure can prevent unexpected artifacts. Finally, they exploit sparse IIR and FIR filters, enabling efficient real-time computation in the CPU.

In this context, we aim to modify the vanilla DAR models so that it can sidestep the aforementioned problem. Inspired by recent works [25], [26], we replace the IIR filters with finite

impulse response (FIR) approximations using the frequency-sampling method (FSM) [27]. Then, each DAR model becomes an FIR filter whose IR can be generated without any recurrent step. We implement differentiable *Filtered Velvet Noise* (FVN) [13], *Advanced Filtered Velvet Noise* (AFVN), and *Feedback Delay Network* (FDN) [28] this way. While the DAR models are not identical to their originals, we show that the differences are negligible. Hence, we can train the ARP estimation networks reliably with the DAR models, then use the original AR models at inference to enjoy their advantages. Our experiments show that the proposed end-to-end framework outperforms the non-end-to-end ARP-matching baselines in terms of both objective evaluations and subjective listening test.

We summarize our contributions as follows:

- We present differentiable FVN, AFVN, and FDN which do not suffer from the bottleneck problem. Our method uses the FSM, which is applicable to any other AR model.
- We show that the end-to-end training enabled by the DAR models gives consistent performance improvement.

The rest of the paper is organized as follows: we review related works in Section II. We develop the FSM in Section III and build the DAR models in Section IV. Our ARP estimation network is explained in Section V. Experimentation setup, and its results are reported in Section VI and VII. We conclude the paper in Section VIII, with supplementary details in Appendix A (ablations), B (baseline methods), and C (proofs).

II. RELATED WORKS

A. Differentiable Digital Signal Processing

Digital signal processing (DSP) and deep learning are closely related. For example, a temporal convolutional network (TCN) [29] is an extension of the Wiener-Hammerstein model [30] and it can model dynamic range compression [31] and reverberation [22]. Direct import of the DSP component to the deep-learning frameworks has recently gained interest since they provide strong structural priors and interpretable representations. For example, a differentiable harmonic-plus-noise model [32] was proposed so that a DNN can be trained together for controllable sound synthesis and timbre transfer [20].

In the case of LTI filters, it is well-known that both an FIR and IIR filter are differentiable and can be directly imported to the deep-learning framework as a convolutional layer and recurrent layer, respectively [16]–[19]. Since the IIR filter, e.g., parametric equalizer (PEQ), bottlenecks the training speed, the FSM [27] was used to accelerate the training [25], [26]. Upon these works, we analyze the FSM’s reliability, present a more general differentiable IIR filter based on the state-variable filter (SVF) [33], [34], and implement the DAR models with it.

B. ARP Estimation

1) *Analysis-synthesis*: The FDN parameters can be obtained from an energy decay relief (EDR) representation from an RIR [11]. A genetic algorithm combined with IIR filter optimization subroutines was also proposed [12]. Using the optimized ARPs as true labels, a support vector regression (SVR) was trained to map room dimensions to the ARPs [15]. FVN, AFVN,

and their ARP estimation algorithm based on linear prediction were also proposed to model late reverberation [13]. However, these methods are not trivial to apply to other tasks, e.g., blind estimation, and AR models.

2) *Blind Estimation*: Previous works [10], [14] formulated this task as a classification of preset or regression of parameters provided in the AR plugin. However, the classification method has a scalability problem. Also, a typical AR plugin’s parameters are much more compact than the actual ARPs, restricting the estimation performance.

3) *Reverberation Parameter Estimation*: Instead of the direct ARP estimation, a two-stage approach with a reverberation parameter (RP) estimation (e.g., reverberation time T_{30} estimation) [35]–[38] followed by an RP-to-ARP task [39]–[41] could be an alternative. However, perceptually different reverberations can be mapped to the same RP, which causes information loss.

C. Modeling Reverberation in the Deep-Learning Framework

A high-order FIR can be directly trained to learn a single RIR [20]. Yet, using this raw representation as a direct estimation target to express various reverberation is highly challenging and inefficient. Instead, recent approaches either train a DNN as a reverberator and control them with conditioning [22], [24] or design a differentiable RIR generator and use a DNN as a parameter estimator [23]. Our method is closely related to the latter since the DAR model and the proposed ARP estimation network act in that way. However, the key difference is that our DAR models are direct imports of the AR models, which bring several benefits discussed above (Section I).

III. FREQUENCY-SAMPLING METHOD FOR DIFFERENTIABLE IIR FILTERS

For any real IIR filter H , its frequency response $H(e^{j\omega})$ is continuous, 2π -periodic, and conjugate symmetric. To obtain its FIR approximation, we *frequency-sample* $H(e^{j\omega})$ at angular frequencies $\omega_k = 2\pi k/N$ where $k = 0, \dots, \lfloor N/2 \rfloor$ [27]. We denote the frequency-sampled filter with subscript N , i.e., H_N .

$$H_N[k] = H(e^{j\omega_k}). \quad (1)$$

Note that the frequency-sampling can also be defined on transfer functions, e.g., $H(z)$ with $z = e^{j\omega_k}$.

Since each sampling is independent, H_N can be generated simultaneously with a parallel processor like GPU. Furthermore, the order of frequency-sampling $(\cdot)_N$ and other basic arithmetic operations does not matter. Therefore, we can frequency-sample an IIR filter by combining frequency-sampled m -sample delays $(z^{-m})_N \in \mathbb{C}^{\lfloor N/2 \rfloor + 1}$ as follows,

$$H_N[k] = \left(\frac{\sum_{m=0}^M \beta_m z^{-m}}{\sum_{m=0}^M \alpha_m z^{-m}} \right)_N [k] = \frac{\sum_{m=0}^M \beta_m (z^{-m})_N[k]}{\sum_{m=0}^M \alpha_m (z^{-m})_N[k]}. \quad (2)$$

Since $(z^{-m})_N[k] = e^{-j2\pi km/N}$, using the widely-used deep-learning libraries, we obtain $(z^{-m})_N$ as a tensor z_m by

$$\text{angle} = 2\pi \text{arange}(N//2+1)/N, \quad (3a)$$

$$z_m = \text{e}^{*\text{*}(-1j*\text{angle}*m)}. \quad (3b)$$

Then, we apply equation (2) to z_0, \dots, z_M with basic tensor operations and obtain every sample of H_N in parallel. A time-domain representation of H_N is a length- N FIR $h_N[n]$, inverse discrete Fourier transform (inverse DFT) of $H_N[k]$, i.e.,

$$h_N[n] = \frac{1}{N} \sum_{k=0}^{N-1} H_N[k] e^{j\omega_k n} (u[n] - u[n-N]) \quad (4)$$

where $u[n]$ is a unit step function. Therefore, using the FSM, we can replace any IIR filter H that causes the bottleneck with an FIR $h_N[n]$ whose convolution can be performed efficiently via Fast Fourier Transform (FFT). In this paper, the “differentiable IIR” filter refers to H_N , which is in fact an FIR filter.

A. Reliability of the Frequency-Sampling Method

A continuous signal is perfectly preserved with sampling only if it is properly band-limited. Notice that Fourier coefficients of a stable LTI filter’s frequency response $H(e^{j\omega})$ are equivalent to its time-flipped IR $h[-n]$. Therefore, every IIR filter has infinite bandwidth and the frequency-sampling causes information loss in the form of *time-aliasing* [42]. That is, the frequency-sampled IR $h_N[n]$ is sum of length- N segments of the original IR $h[n]$.

$$h_N[n] = \sum_{m=0}^{\infty} h[mN + n] (u[n] - u[n-N]). \quad (5)$$

Since the energy of every stable IIR filter’s IR decays over time, more frequency-sampling points N give less time-aliasing, i.e., a closer approximation. Therefore, we can use the differentiable filter H_N in place of the original H to match a target response H_t . We elaborate this with following analytical results.

1) *Time-aliasing Error*: If H has M distinct poles where each of them $\nu_i \in \mathbb{C}$ has multiplicity $r_i \in \mathbb{N}$, the time-aliasing error asymptotically decreases as N increases as follows,

$$\|H - H_N\|_2 = \sum_{i=1}^M O(N^{r_i-1} |\nu_i|^N). \quad (6)$$

2) *Loss Error*: The triangle inequality indicates that the loss error caused by the FSM is bounded to the time-aliasing error.

$$|\|H_t - H\|_2^2 - \|H_t - H_N\|_2^2| \leq \|H - H_N\|_2^2. \quad (7)$$

3) *Loss Gradient Error*: The loss gradient error has similar asymptotic behavior to the time-aliasing error as follows,

$$\left| \frac{\partial}{\partial p} \|H_t - H\|_2^2 - \frac{\partial}{\partial p} \|H_t - H_N\|_2^2 \right| = \sum_{i=1}^M O(N^{3r_i-1} |\nu_i|^N)$$

where p is a parameter. Refer to Appendix A-C for the empirical analysis on this topic. For the proofs, refer to Appendix C.

B. Differentiable Dense IIR Filter with State-variable Filters

Since arbitrary IIR filter can be expressed as serially cascaded biquads (second-order IIR filters), we can obtain a differentiable IIR filter \tilde{H} as a product of frequency-sampled biquads $(H_i)_N$.

$$\tilde{H}[k] = \prod_i (H_i)_N[k] = \prod_i \left(\frac{\sum_{m=0}^2 \beta_{i,m} z^{-m}}{\sum_{m=0}^2 \alpha_{i,m} z^{-m}} \right)_N [k]. \quad (9)$$

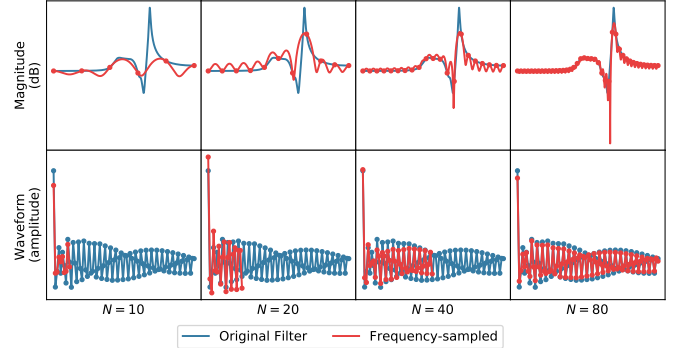


Fig. 2. The FSM with a various number of sampling points N . Here, H is an 8th-order IIR filter. Blue curves represent its magnitude response $|H(e^{j\omega})|$ (top row) and IR $h[n]$ (bottom row). Red curves are the magnitude response and IR of the frequency-sampled filter H_N . The response error happens in-between the samples and gets smaller as N increases. In the time domain, the FIR approximation $h_N[n]$ gets longer, and the time-aliasing error decreases.

Moreover, we use the *state variable filter* (SVF) parameters $f_i, R_i, m_i^{\text{LP}}, m_i^{\text{BP}}$, and m_i^{HP} to express each biquad as follows,

$$\beta_{i,0} = f_i^2 m_i^{\text{LP}} + f_i m_i^{\text{BP}} + m_i^{\text{HP}}, \quad (10a)$$

$$\beta_{i,1} = 2f_i^2 m_i^{\text{LP}} - 2m_i^{\text{HP}}, \quad (10b)$$

$$\beta_{i,2} = f_i^2 m_i^{\text{LP}} - f_i m_i^{\text{BP}} + m_i^{\text{HP}}, \quad (10c)$$

$$\alpha_{i,0} = f_i^2 + 2R_i f_i + 1, \quad (10d)$$

$$\alpha_{i,1} = 2f_i^2 - 2, \quad (10e)$$

$$\alpha_{i,2} = f_i^2 - 2R_i f_i + 1. \quad (10f)$$

We prefer to use the SVF parameters rather than the biquad coefficients due to the following reasons.

- *Interpretability*. Each SVF has lowpass H_i^{LP} , bandpass H_i^{BP} , and highpass filter H_i^{HP} . They share a resonance R_i and cutoff parameter $f_i = \tan(\pi\omega_i/\omega_s)$ where ω_i is their cutoff frequency and ω_s is the sampling rate. The filter outputs are multiplied with gains m_i^{LP} , m_i^{BP} , and m_i^{HP} and then summed. This interpretability comes without any generality loss since an SVF can express any biquad [34].
- *Simple Activation Functions*. The SVF parameters have simpler stability conditions, $R_i > 0$ and $f_i > 0$, than the biquad coefficients [19], which leads to simpler activation function design. Refer to Section V-C for details.
- *Better Performance*. We found that our ARP estimation networks performed better when they estimate the SVF parameters rather than the biquad coefficients. Refer to Appendix A-B for the comparison results.

From now on, we denote each SVF-parameterized biquad with a superscript H_i^{SVF} and call it simply “SVF”.

C. Differentiable Parametric Equalizer

A low-shelving H^{LS} , peaking H^{Peak} , and high-shelving filter H^{HS} are widely used audio filters. Each of them can be obtained using the SVF $H^{\text{SVF}}(f, R, m^{\text{LP}}, m^{\text{BP}}, m^{\text{HP}})$ as follows [33],

$$H^{\text{LS}}(f, R, G) = H^{\text{SVF}}(f, R, 1, 2R\sqrt{G}, G), \quad (11a)$$

$$H^{\text{Peak}}(f, R, G) = H^{\text{SVF}}(f, R, 1, 2RG, 1), \quad (11b)$$

$$H^{\text{HS}}(f, R, G) = H^{\text{SVF}}(f, R, G, 2R\sqrt{G}, 1). \quad (11c)$$

Here, G is a new parameter that gives $20 \log_{10}(G)$ dB gain. A parametric equalizer (PEQ) is serial composition of such filters. Following the recent works [25], [26], we use one low-shelving, one high-shelving, and $K - 2$ peaking filters.

$$H^{\text{PEQ}}(z) = H^{\text{LS}}(z)H^{\text{HS}}(z) \prod_{i=1}^{K-2} H_i^{\text{Peak}}(z). \quad (12)$$

Same as the IIR filter case, frequency-sampling the components and multiplying them results in a differentiable PEQ H_N^{PEQ} .

IV. DIFFERENTIABLE ARTIFICIAL REVERBERATION

In this section, we derive differentiable FVN, AVFN, and FDN. We first briefly review the original AR models. Then, we obtain their DAR counterparts by replacing the IIR components with FIRs using the FSM. Also, we slightly modify the original models for efficient training, plausible reverberation, and better overall estimation performance.

A. Differentiable Filtered Velvet Noise

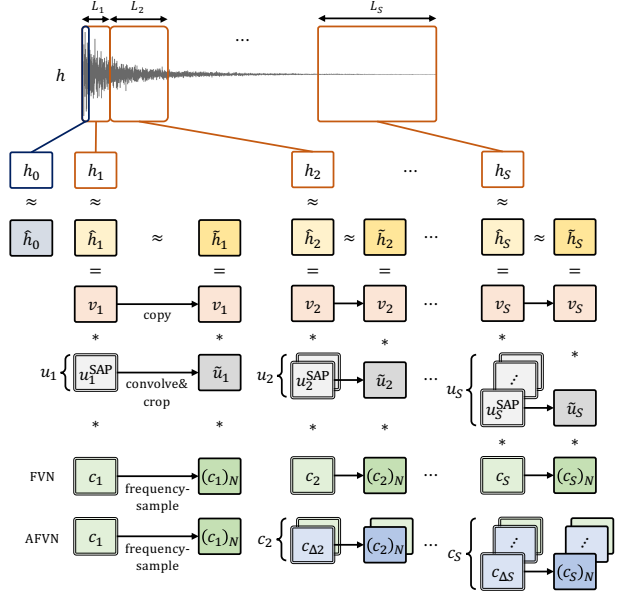
1) *Filtered Velvet Noise*: One can divide an RIR $h[n]$ into S segments (see Figure 3a). As reverberation is mostly stochastic, we can model each length- L_i segment $h_i[n]$ with a source noise $s_i[n]$ “colored with” a filter C_i . When we use *velvet noise* for each source, this source-filter model becomes *Filtered Velvet Noise* (FVN) [13], [43], [44]. The velvet noise $v_i[n]$ is sparse; in every length- T_i interval, it contains a single nonzero sample ± 1 with random sign/position such that its time-domain convolution is highly efficient. Moreover, an allpass filter U_i is introduced to smooth each source and make plausible sound. Finally, an deterministic (bypass) FIR $\hat{h}_0[n]$ models the direct arrival and early reflection. Then, an IR of FVN $\hat{h}[n]$ becomes

$$\hat{h}[n] = \hat{h}_0[n] + \sum_{i=1}^S \underbrace{v_i[n - d_i] * u_i[n] * c_i[n]}_{\hat{h}_i[n - d_i]} \quad (13)$$

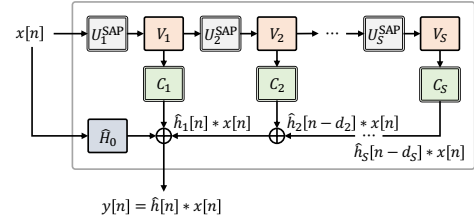
where each d_i is a delay for the segment alignment ($d_1 = 0$). In practice, each allpass filter U_i is composed with Schroeder allpass filters (SAPs, $U_{i,j}^{\text{SAP}}(z) = (1 + \gamma_{i,j}z^{-\tau_{i,j}}) / (\gamma_{i,j} + z^{-\tau_{i,j}})$), where $\tau_{i,j}$ is a delay-line length and $\gamma_{i,j}$ is a feed-forward/back gain) for efficiency [45]. A low-order dense IIR filter is used as each coloration filter C_i .

2) *Differentiable Implementation*: We modify each FVN component to obtain differentiable FVN (refer to Figure 3a).

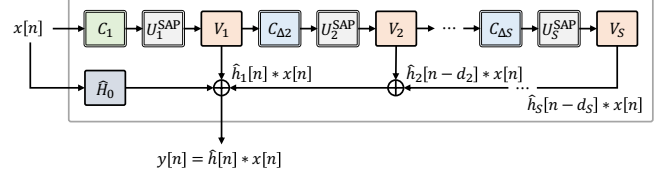
- *Velvet filters*. To batch the IR segments, we use the same segment lengths L_1, \dots, L_S and average pulse distance values T_1, \dots, T_S for every target IR.
- *Allpass filters*. We tune and fix the allpass filter parameters jointly with the velvet filter parameters to avoid perceptual artifacts, e.g., discontinuous and rough sound, while being computationally efficient. Since we fixed the filter, instead of the FSM, we simply crop its IR to obtain an FIR $\tilde{u}_i[n]$.
- *Coloration filters*. We model C_i with K serial SVFs, i.e., $C_i(z) = \prod_{k=1}^K C_{i,k}^{\text{SVF}}(z)$. We frequency-sample each filter $C_i(z)$ and convert it into a length- N FIR $(c_i)_N[n]$ so that we can train our network to estimate its parameters.



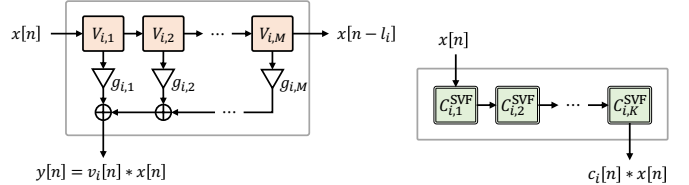
(a) Modified FVN, AVFN's RIR approximation, and their differentiable implementation strategy.



(b) Modified FVN in the time domain.



(c) Modified AVFN in the time domain.



(d) Each velvet filter V_i .

(e) Each coloration filter C_i .

Fig. 3. FVN, AVFN, and their differentiable versions. (a) FVN and AVFN divide a target RIR $h[n]$ into segments $h_i[n]$ and approximate each segment with a velvet noise v_i filtered with an allpass filter U_i and a coloration filter C_i . We obtain the differentiable FVN and AVFN by converting the IIR filters U_i and C_i into FIR filters \tilde{u}_i and $(c_i)_N$. Each IIR filter is emphasized with a double border box. (b) Modified FVN. To retain a sharp transient, we insert each SAP before its corresponding velvet filter. For each velvet filter V_i , the output denoted with a down arrow is a convolution of the input and the velvet noise $v_i[n]$. The other output denoted with a right arrow is a L_i -sample-delayed input. Refer to [13] for more details. (c) The same modification is performed to the AVFN model. (d) For both FVN and AVFN, each velvet filter V_i is divided into smaller velvet filters $V_{i,1}, \dots, V_{i,M}$ assigned with gains $g_{i,1}, \dots, g_{i,M}$. This modification is equivalent to dividing each velvet segment $v_i[n]$ into smaller segments $v_{i,1}[n], \dots, v_{i,M}[n]$ and multiplying them with $g_{i,1}, \dots, g_{i,M}$. (e) The i^{th} coloration filter C_i in the time domain, which is serial connection of the SVF-parameterized biquads $C_{i,1}^{\text{SVF}}, \dots, C_{i,K}^{\text{SVF}}$.

Therefore, IR of the differentiable FVN $\tilde{h}[n]$ becomes

$$\tilde{h}[n] = \hat{h}_0[n] + \text{overlap-add}\{\underbrace{v_i[n] * \tilde{u}_i[n] * (c_i)_N[n]}_{\tilde{h}_i[n]}\}. \quad (14)$$

Since every component $v_i[n]$, $\tilde{u}_i[n]$, and $(c_i)_N[n]$ is an FIR, we can compute each segment $\tilde{h}_i[n] = v_i[n] * \tilde{u}_i[n] * (c_i)_N[n]$ efficiently by convolving the FIRs in the frequency domain, i.e., zero-padding followed by FFT, multiplication, then IFFT. Finally, we overlap-add all the segments and add the deterministic FIR $\hat{h}_0[n]$ to obtain the full IR $\tilde{h}[n]$. The overlap-add can be implemented with a transposed convolution layer.

3) *Modifications to the Original Model*: FVN was initially designed for the analysis-synthesis of late reverberation; it used the ground-truth direct arrival and early reflection cropped from the RIR and modeled only the late part. However, we also aim to solve the blind estimation where we must estimate the entire RIR. To this end, we modify the original model as follows.

- *Finer segment gain*. We divide each velvet segment $v_i[n]$ into M smaller segments $v_{i,1}[n], \dots, v_{i,M}[n]$ multiplied with gains $g_{i,1}, \dots, g_{i,M}$. Figure 3d shows the resulting velvet filter V_i in the time domain.
- *Cumulative allpass*. The original model smoothes every velvet noise with the same allpass filter. This is undesirable in our context since it could smear the direct arrival and early reflections. Instead, we gradually cascade the SAPs to obtain each allpass filter $U_i(z) = \prod_{j=1}^i U_j^{\text{SAP}}(z)$ so the earlier segments are less smeared than the later ones. As shown in Figure 3b, this modification can be implemented in the time domain by inserting each SAP U_j^{SAP} before the corresponding velvet filter V_j .
- *Shorter deterministic FIR*. With the above changes, the stochastic segments can fit the early RIR to some extent. Therefore, we shorten the early deterministic FIR $\hat{h}_0[n]$.

Refer to Appendix A-A for the evaluation of the modifications.

4) *Model Configuration Details*: Exact configurations of our FVN used for the experiments are as follows.

We generated 2.5 seconds of IR (48kHz sampling rate, total $L = 120k$ samples) with FVN. We used $S = 20$ non-uniform velvet segments whose lengths L_i are $L/40, L/20$, and $L/10$ for 10, 5, and 5 segments, respectively, and their average pulse distances were set to $\mathbf{T} = [10, 20, 35, 50, 65, 90, 120, 135, 180, 220, 270, 320, 370, 420, 480, 540, 610, 680, 750, 820]$. The SAPs U_j^{SAP} were forced to have gains $\gamma_j = 0.75 + 0.01j$ and delay lengths $\tau = [23, 48, 79, 109, 113, 127, 163, 191, 229, 251, 293, 337, 397, 421, 449, 509, 541, 601, 641, 691]$. Each velvet segment had $M = 4$ sub-segment gains and filtered with $K = 8$ SVFs. We frequency-sampled the coloration filters with $N = 4k$ points. The length of the deterministic FIR $h_0[n]$ was set to 50. We set the gain $\mathbf{g} \in \mathbb{R}^{S \times M}$, SVF parameters $\mathbf{f}, \mathbf{R}, \mathbf{m}^{\text{LP}}, \mathbf{m}^{\text{BP}}, \mathbf{m}^{\text{HP}} \in \mathbb{R}^{S \times K}$, and the bypass FIR $\mathbf{h}_0 \in \mathbb{R}^Z$ to estimation targets (total 930 ARPs). The time-domain FVN \hat{H} requires 2166 floating point operations per sample (FLOPS).

B. Differentiable Advanced Filtered Velvet Noise

Since frequency-dependent decay of reverberation is gradual, one can model each coloration filter C_i as an initial coloration

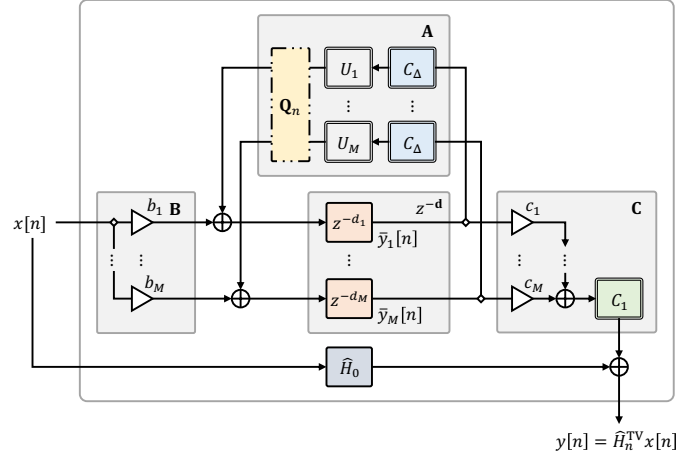


Fig. 4. Our modified FDN in the time domain. We restrict the fully general filter matrices to accelerate the training and obtain an efficient and controllable model. We simplify \mathbf{B} and \mathbf{C} to have only one coloration filter C_1 and use the same C_Δ for all feedback loops. A time-varying mixing matrix \mathbf{Q}_n and allpass filters \mathbf{U} are introduced to use FDN with small M (i.e., fast training) with minimal reverberation quality loss.

filter C_1 cascaded with delta-coloration filters $C_{\Delta 2}, \dots, C_{\Delta i}$.

$$C_i(z) = C_1(z) \prod_{j=2}^i C_{\Delta j}(z). \quad (15)$$

FVN with this modification is called *Advanced Filtered Velvet Noise* (AVFN) [13]. The delta filters' orders $\Delta K_2, \dots, \Delta K_S$ are set lower than the initial filter's K_1 for the efficiency. See Figure 3c for its time-domain implementation. We used $K_1 = 8$ and $K_\Delta = K_{\Delta 2} = \dots = K_{\Delta S} = 2$ in the experiments. This results in a total of $\bar{K} = K_1 + (S-1)K_\Delta = 46$ SVFs. Other settings are same with the FVN. This AVFN has 360 ARPs to estimate and its time-domain model \hat{H} requires 1511 FLOPS.

C. Differentiable Feedback Delay Network

1) *Feedback Delay Network*: The most widely used class of AR models is the *delay network*, which recursively interconnects long delay lines [4]. Among numerous delay network models, we implement *Feedback Delay Network* (FDN) [28] differentiably since it can express any other delay networks [46], [47]. Difference equation of the FDN is as follows (we omit the bracket notation for the filtering),

$$y[n] = \mathbf{C}^T \bar{y}[n] + \hat{H}_0 x[n], \quad (16a)$$

$$\bar{y}[n + \mathbf{d}] = \mathbf{A} \bar{y}[n] + \mathbf{B} x[n]. \quad (16b)$$

That is, an input $x[n]$ is distributed and filtered with \mathbf{B} , then go through \mathbf{d} -sample parallel delay lines which are recursively interconnected to themselves through a mixing filter matrix \mathbf{A} . The delay line outputs $\bar{y}[n]$ are filtered and summed with \mathbf{C} . We add a bypass signal filtered with \hat{H}_0 , resulting in an output $y[n]$. Transfer function of the FDN can be written as follows,

$$\hat{H}(z) = \mathbf{C}(z)^T (\mathbf{D}^{-1}(z) - \mathbf{A}(z))^{-1} \mathbf{B}(z) + \hat{H}_0(z). \quad (17)$$

Here, $\mathbf{D}(z) = \text{diag}(z^{-\mathbf{d}})$ is a diagonal transfer function matrix (TFM) of shape $M \times M$ for the delay lines, i.e., $\mathbf{D}_{ii}(z) = z^{-d_i}$.

$\mathbf{B}(z)$, $\mathbf{C}(z)$, and $\mathbf{A}(z)$ are input, output, and feedback TFM of shape $M \times 1$, $1 \times M$, and $M \times M$, respectively.

2) *Differentiable Implementation*: The FDN components are recursively interconnected such that one cannot divide its IR into independent segments and generate them in parallel like we did with the FVN and AVFN. Instead, we frequency-sample its entire transfer function $\hat{H}(z)$ to obtain differentiable FDN $\tilde{H} = \hat{H}_N$, which is equivalent to a composition of individually frequency-sampled TFM (FSTFMs).

$$\tilde{h}[n] = \text{IFFT} \left\{ \mathbf{C}_N^T (\mathbf{D}_N^{-1} - \mathbf{A}_N)^{-1} \mathbf{B}_N + (\hat{H}_0)_N \right\}. \quad (18)$$

Here, $\mathbf{D}_N = \text{diag}((z^{-\mathbf{d}})_N) \in \mathbb{C}^{M \times M \times \lfloor N/2+1 \rfloor}$ is an $M \times M$ diagonal FSTFM of \mathbf{D} , i.e., $(\mathbf{D}_N)_{ii} = (z^{-d_i})_N \in \mathbb{C}^{\lfloor N/2+1 \rfloor}$. Likewise, we can build \mathbf{B}_N , \mathbf{C}_N , and \mathbf{A}_N whose elements are frequency-sampled transfer functions of their original TFM \mathbf{B} , \mathbf{C} , and \mathbf{A} , respectively. Each FSTFM is a batch of $\lfloor N/2+1 \rfloor$ matrices; the matrix multiplications and inversions of equation (18) can be performed in parallel.

3) *Restrictions to the General Model*: Now it is obvious that we can derive a differentiable approximation of any FDN model (hence any delay network model). However, when following the general practice that uses many parallel delay lines (e.g., $M = 16$) for a high-quality reverberation, its differentiable model's FSTFMs consume too much memory, and their multiplications and inversions bottleneck the training speed. To tackle this, we reduce M and modify the components to make FDN plausible with low M . Refer to Figure 4 for its time-domain illustration.

- *Pre and Post Filter Matrix*. Following most previous works [11], [47], [48], the pre filter matrix \mathbf{B} is set to a (constant) gain vector \mathbf{b} . The post filter matrix \mathbf{C} is a combination of a gain vector \mathbf{c} and a common filter C_1 , i.e., $\mathbf{C} = C_1 \mathbf{c}$. The common filter C_1 is composed of serial K_{C_1} SVFs.
- *Feedback Filter Matrix*. While most FDN model combines channel-wise parallel delta-coloration (absorption) filters \mathbf{C}_Δ and an inter-channel mixing matrix \mathbf{Q} to compose the feedback filter matrix $\mathbf{A} = \mathbf{Q} \mathbf{C}_\Delta$. Additionally, we insert channel-wise allpass filters \mathbf{U} and introduce *time-variance* by modulating the mixing matrix \mathbf{Q} . This results in the time-varying feedback filter matrix $\mathbf{A}_n = \mathbf{Q}_n \mathbf{U} \mathbf{C}_\Delta$.
- *Allpass Filters*. For each FDN with SAPs inserted in its feedback loop, an equivalent FDN without the SAPs exists and has more channels [47]. Therefore, our modification is a way to compress the number of channels while retaining the echo density build-up speed [49]. Each channel has serial K_U SAPs. Unlike the FVN and AVFN case, we estimate the SAP gains $\gamma \in \mathbb{R}^{M \times K_U}$ with the estimation network and frequency-sample the allpass filter matrix \mathbf{U} for the differentiable model.
- *Time-varying Mixing Matrix*. We further reduce the audible artifacts by modulating the stationary poles with the time-varying mixing matrix, which is set to $\mathbf{Q}_n = \mathbf{Q}_0 \mathbf{R}^n$ where \mathbf{Q}_0 is a Householder matrix and \mathbf{R} is a tiny rotational matrix constructed from a random matrix [46], [47]. Since the FSM is only applicable to LTI filters, we fix the mixing matrix to \mathbf{Q}_0 when obtaining the differentiable model.
- *Absorption Filters*. We use the same absorption filter C_Δ for every channel. Since the mixing matrix \mathbf{Q}_n is always

unitary, our FDN becomes stable when C_Δ has magnitude response less than 1 [47]. We achieve this by using a PEQ with additional constraints (see Section V-C) as C_Δ .

• *Bypass FIR*. We use a length- Z FIR $h_0[n]$ for the bypass.

We summarize the modifications. The difference equation of our time-varying FDN \hat{H}_n^{TV} is

$$y[n] = C_1 \mathbf{c}^T \bar{\mathbf{y}}[n] + H_0 x[n], \quad (19a)$$

$$\bar{\mathbf{y}}[n + \mathbf{d}] = \mathbf{Q}_n \mathbf{U} \mathbf{C}_\Delta \bar{\mathbf{y}}[n] + \mathbf{b} x[n]. \quad (19b)$$

The transfer function of its LTI approximation $\hat{H}(z)$ is given as equation (17) with the restrictions $\mathbf{B}(z) = \mathbf{b}$, $\mathbf{C}(z) = C_1(z) \mathbf{c}$, and $\mathbf{A}(z) = \mathbf{Q}_0 \text{diag}(\mathbf{U}_N(z) \odot \mathbf{C}_\Delta(z))$. Hence, the IFFT of

$$(C_1)_N \mathbf{c}^T (\mathbf{D}_N^{-1} - \mathbf{Q}_0 \text{diag}(\mathbf{U}_N \odot (\mathbf{C}_\Delta)_N))^{-1} \mathbf{b} \quad (20)$$

summed with the bypass FIR $\hat{h}_0[n]$ results in our differentiable FDN's IR $\tilde{h}[n]$.

4) *Model Configuration Details*: We used $M = 6$ delay lines with fixed delay lengths $\mathbf{d} = [233, 311, 421, 461, 587, 613]$. We used $K_U = 4$ SAPs for each delay channel. We fixed the SAP delays to $\boldsymbol{\tau} = [[131, 151, 337, 353], [103, 173, 331, 373], [89, 181, 307, 401], [79, 197, 281, 419], [61, 211, 257, 431], [47, 229, 251, 443]]$. Our rotational matrix satisfies $\mathbf{R}^{30k} = \mathbf{I}$ so that the mixing matrix \mathbf{Q}_n has a period of 0.625 second. Both post C_1 and absorption filter C_Δ have $K_{C_1} = K_{C_\Delta} = 8$ components. We used the FSM with $N = 120k$ samples. The order of the bypass FIR H_0 is $Z = 100$. The post filter parameters \mathbf{f}_{C_1} , \mathbf{R}_{C_1} , $\mathbf{m}_{C_1}^{\text{LP}}$, $\mathbf{m}_{C_1}^{\text{BP}}$, $\mathbf{m}_{C_1}^{\text{HP}} \in \mathbb{R}^{1 \times K_{C_1}}$, feedback filter parameters \mathbf{f}_{C_Δ} , \mathbf{R}_{C_Δ} , $\mathbf{G}_{C_\Delta} \in \mathbb{R}^{M \times K_{C_\Delta}}$, pre/post gain vectors \mathbf{b} , $\mathbf{c} \in \mathbb{R}^{M \times 1}$, SAP gain vector $\boldsymbol{\gamma} \in \mathbb{R}^{M \times K_U}$, and the bypass FIR $\mathbf{h}_0 \in \mathbb{R}^Z$ are the estimation targets (total 200 ARPs). The resulting time-domain model \hat{H} and the time-varying model \hat{H}_n^{TV} consume 889 and 1285 FLOPs, respectively.

V. ARTIFICIAL REVERBERATION PARAMETER ESTIMATION WITH A DEEP NEURAL NETWORK

The details of our ARP estimation network are as follows. As shown in Figure 1, it transforms single channel audio input (either RIR or reverberant speech) into a shared latent \mathbf{z} with the model/task-agnostic encoder. Then, each ARP-groupwise layer projects the latent \mathbf{z} into an ARP tensor \mathbf{P}_i .

A. AR-Model-agnostic Encoder

The encoder first transforms the input (2.5 seconds, 48kHz sampling rate, total 120k samples) into a log-frequency log-magnitude spectrogram. Next, the spectrogram goes through five two-dimensional convolutional layers, each followed by a rectified linear unit (ReLU) activation. We apply gated recurrent units [50] along with the frequency axis regarding the channels as features (FGRU) and the time axis regarding the channels and frequencies as features (TGRU), widening the receptive field. Finally, we apply two dense layers with the same input/output size followed by layer normalization [51] and ReLU, resulting in the two-dimensional shared latent \mathbf{z} .

Detailed encoder configurations are as follows. We used 1024 FFT size, 128 hop size, and Hann window for the spectrogram. We set the convolutional layers as follows. Channel: 64, then

128 afterwards. Kernel size (in frequency-time order): (7, 5), then (5, 5) afterwards. Stride: (1, 2), (2, 1), (2, 2), (2, 2), and (1, 1). The FGRU and TGRU are bidirectional and have 2 and 1 layer(s) with 128 and 64 hidden features, respectively. This setting results in the encoder with about 7M parameters.

B. ARP-groupwise Projection Layers

Now we aim to transform the two-dimensional shared latent $\mathbf{z} \in \mathbb{R}^{M_1 \times M_2}$ into each ARP tensor $\mathbf{P}_i \in \mathbb{R}^{N_{i,1} \times N_{i,2}}$, which is at most two-dimensional. We treat the one-dimensional tensors also as two-dimensional by setting $N_{i,1} = 1$ or $N_{i,2} = 1$. Then, we compose each projection layer with two axis-by-axis shape-matching dense layers. That is, we first transpose and apply an M_1 -to- $N_{i,1}$ dense layer to \mathbf{z} to obtain an $M_2 \times N_{i,1}$ tensor. Then, applying another transpose and M_2 -to- $N_{i,2}$ dense layer to the intermediate tensor gives the desired shape. We do not use nonlinear activation between the dense layers. This approach factorizes a single large $M_1 M_2$ -to- $N_{i,1} N_{i,2}$ dense layer into two smaller layers, reducing the number of parameters from $N_{i,1} N_{i,2} (M_1 M_2 + 1)$ to $N_{i,1} (M_1 + 1) + N_{i,2} (M_2 + 1)$.

C. Nonlinear Activation Functions and Bias Initialization

Each ARP group has different stability conditions and desired distribution. To satisfy these, we attach a nonlinear activation to each projection layer and initialize the last dense layer's bias as follows. Here, x denotes a pre-activation element.

1) Nonlinear Activation Functions:

- For the resonance \mathbf{R} of the SVF, we use a scaled softplus $\zeta(x) = \log(1+e^x)/\log(2)$ to center the initial distribution at 1 and satisfy the stability condition $\mathbf{R} > \mathbf{0}$.
- For cutoff \mathbf{f} also have the same stability condition $\mathbf{f} > \mathbf{0}$. However, instead of the softplus, we use $\tan(\pi\sigma(x)/2)$ where $\sigma(x) = 1/(1+e^{-x})$ is a logistic sigmoid. With this activation, $\sigma(x) = 0$ and 1 represent cutoff frequency of 0Hz and half of the sampling rate, respectively.
- The delta-coloration PEQ C_Δ inside the FDN must satisfy the stability condition $|C_\Delta(e^{j\omega})| < 1$. To achieve this, we use $10^{-\zeta(x)}$ for the component gain \mathbf{G} . Also, the shelving filters' resonances should satisfy $\mathbf{R} > \sqrt{2}/2$ to prevent their magnitude responses to “spike” over 1. Therefore, we add $\sqrt{2}/2$ after the softplus activation.
- For the feed-forward/back gains γ of channel-wise allpass filters \mathbf{U} inside FDN, we use sigmoid activation $\sigma(x)$.

2) Bias Initialization:

- We initialize bias of the \mathbf{f} projection layer to $\sigma^{-1}(2\omega_k/\omega_s)$ where each ω_k is desired initial cutoff frequency of k^{th} SVF. We set $\omega_k = \omega_{\min} (\omega_{\max}/\omega_{\min})^{(k-1)/(K-1)}$ such that the frequencies are equally spaced in the logarithmic scale from $\omega_{\min} = 40\text{Hz}$ to $\omega_{\max} = 12\text{kHz}$. To the SVFs inside the AVFN's initial and delta-coloration filters, we perform a random permutation to the frequency index k and obtain a new index \bar{k} . This prevents SVFs for the latter segments having higher initial cutoff frequencies.
- Decoder biases for the SVF mixing coefficients \mathbf{m}^{LP} , \mathbf{m}^{BP} , and \mathbf{m}^{HP} are initialized to 1, 2, and 1, respectively, such that each SVF's initial magnitude response slightly deviate

from 1. This prevents the coloration filters' responses and the estimation network loss gradients to vanish or explode.

- For the PEQ gains \mathbf{G} of the FDN's delta-coloration filters, we set each of their biases to -10 such that the initially generated IRs have long enough reverberation time.

D. Loss Function

1) *Match Loss*: We utilize a multi-scale spectral loss from [20], and define a match loss as

$$\mathcal{L}_{\text{MATCH}}(h, \tilde{h}) = \sum_i \left\| |\text{STFT}_i(h)| - |\text{STFT}_i(\tilde{h})| \right\|_1 \quad (21)$$

i denotes STFT with different FFT sizes. We use the FFT sizes of 256, 512, 1024, 2048, and 4096, hop sizes of 25% of the respective FFT sizes, and Hann windows. Each spectrogram's frequency axis is log-scaled like the encoder's spectrogram.

2) *Regularization*: We additionally apply a regularization to reduce time-aliasing of the estimation. As shown in equation (6) and (8), pole radii of each SVF affects the reliability of the frequency-sampled one (hence DAR model) and its parameter estimator. Since each SVF's IR $(c_{i,k}^{\text{SVF}})_N[n]$ can be computed, we encourage reducing its pole radii by penalizing the IR's decreasing speed. Each decreasing speed $\gamma_{i,k}$ is calculated by the ratio of the average amplitude of first and last n_0 samples of $(c_{i,k}^{\text{SVF}})_N[n]$. We fix n_0 to $N/8$. Then, each $\gamma_{i,k}$ is weighted with a softmax function along the SVF-axis to penalize higher $\gamma_{i,k}$ more. Sum of the weighted decreasing speed values results in the regularization loss \mathcal{L}_{REG} as follows,

$$\gamma_{i,k} = \frac{\sum_{n=N-n_0}^N |(c_{i,k}^{\text{SVF}})_N[n]|}{\sum_{n=0}^{n_0} |(c_{i,k}^{\text{SVF}})_N[n]|}, \quad (22a)$$

$$\mathcal{L}_{\text{REG}} = \sum_{i=1}^S \frac{\sum_{k=1}^K \gamma_{i,k} e^{\gamma_{i,k}}}{\sum_{j=1}^K e^{\gamma_{i,j}}}. \quad (22b)$$

We omit the regularization loss for the FDN networks since with FDN the time-aliasing is inevitable to match the target with reverberation time longer than the number of frequency-sampling points N . Therefore, our full loss function \mathcal{L} is

$$\mathcal{L}(h, \tilde{h}) = \mathcal{L}_{\text{MATCH}}(h, \tilde{h}) + \beta \mathcal{L}_{\text{REG}}(\mathbf{c}_N^{\text{SVF}}) \quad (23)$$

where $\beta = 1$ for the FVN and AVFN and $\beta = 0$ for the FDN.

VI. EXPERIMENTAL SETUP

A. Data

1) *Room Impulse Response*: We collected real-world RIR measurements from various dataset including OpenAIR [52] and ACE Challenge [53]. We split a total of 1835 RIRs into the validation (836) and test set (999), ensuring that each of them consists of RIRs from different rooms.

For the training, we synthesized RIRs with shoebox room simulations based on the image-source method [54], [55]. To reflect various acoustic environments, we randomized various simulation parameters for each simulation, such as room size, each wall's frequency-dependent absorption coefficient, and source and microphone position. We tuned the randomization scheme to match the training dataset to the validation set in terms of the RP statistics. We generated a total of 200k RIRs.

TABLE I
ARP ESTIMATION RESULTS ON VARIOUS TASKS AND DAR MODELS.

MODEL	TASK	TRAIN TEST	$10^{-1}\mathcal{L}_{\text{MATCH}}$	T ₃₀ (%)		DRR (dB)		C ₅₀ (dB)		SUBJ
				FULL	FREQ	FULL	FREQ	FULL	FREQ	
FVN	AS	AS	1.236 1.236	1.79	1.89	4.26	4.20	0.92	0.94	0.56 0.60
		BE	1.436 1.437	9.23	9.12	11.60	11.73	2.04	2.01	0.93 0.93
		BOTH	1.351 1.350	2.88	2.92	8.84	8.74	1.38	1.39	0.64 0.67
		AS	1.450 1.450	12.96	13.06	16.41	16.39	2.27	2.30	0.99 0.98
	BEP	ASP	1.915 1.918	51.07	50.99	46.79	47.47	3.42	3.38	4.97 4.93
		BEP	1.869 1.869	36.70	36.76	32.09	32.60	3.21	3.26	3.64 3.60
AFVN	AS	AS	1.275 1.277	4.06	4.77	9.67	9.96	1.61	1.59	3.72 3.64
		BE	1.436 1.437	9.65	9.57	12.50	12.47	2.30	2.31	4.20 4.16
		BOTH	1.407 1.407	6.51	6.16	9.11	9.07	1.36	1.39	4.16 4.19
		AS	1.442 1.441	10.11	9.91	12.52	12.41	2.31	2.28	4.58 4.68
	BEP	ASP	1.986 1.986	29.99	29.92	38.46	38.11	3.51	3.55	5.67 5.60
		BEP	1.757 1.758	29.36	29.04	28.03	28.10	3.10	3.06	5.08 5.05
FDN	AS	AS	1.277 1.307 1.334	5.60	5.93	8.47	11.86 12.48	11.59	1.78 1.81 1.71	3.80 3.93 3.83
		BE	1.428 1.436 1.484	15.04	15.38	13.26	18.08 18.10	15.62	4.16 4.16 3.93	6.76 6.77 6.56
		BOTH	1.386 1.387 1.399	7.34	7.34	7.43	9.06	9.06	2.06 2.06 2.28	5.36 5.36 5.45
		AS	1.436 1.439 1.453	15.08	15.09	13.91	16.19 16.23	15.60	3.74 3.74 3.90	6.63 6.62 6.69
	BEP	ASP	2.065 2.065 2.076	55.27 55.17	46.20	56.13 56.12	55.35	7.85 7.85 8.01	8.56 8.56 8.67	4.05 4.05 4.06
		BEP	2.121 2.121 2.131	40.40	40.40	41.87	30.99 30.99	30.90	3.45 3.45 3.45	5.26 5.26 5.31
DNN	AS		1.032		2.68	5.61		3.94	4.79	0.96
	BE		1.371		12.63	17.34		6.42	6.04	1.72
RANDOM RIR PAIRS			3.145		69.07	70.74		5.29	6.74	6.06
HIDDEN REFERENCE			—		—	—		—	—	— 86.5±1.9

In addition, we pre-processed each RIR as following.

- We removed the unnecessary pre-onset part of the RIR so that it immediately starts with the direct arrival. We detected the onset using the mean-over-time method [56].
- Following the recent DRR augmentation method [57], we multiplied random gain sampled from $\mathcal{U}(-12\text{dB}, 3\text{dB})$ to the first 5ms of each train RIR. This slightly reduces the average DRR of the training set and matches the validation set. We omitted this procedure at the evaluation/test.
- Finally, we normalized the RIR to have the energy of 1.

2) *Reverberant Speech*: We used VCTK [58] for dry speech. We split it into the train (61808), validation (21608), and test (4912) set so that each set is composed of the speech recordings from different speakers. We sampled an RIR and a dry speech sample from the respective datasets and convolved them to generate reverberant speech. We random-cropped 2.5-second segment from it for the input.

B. Training

We trained each network Φ with every proposed DAR model for the three tasks: analysis-synthesis (AS), blind estimation (BE), and both tasks (BOTH). For the both-performing ones, we fed an RIR or reverberant speech in a 50-50% probability.

We set the initial learning rate to 10^{-4} for FVN and AVFN and 10^{-5} for FDN. We used Adam optimizer [59]. For FDN, gradients were clipped to ± 10 for stable training. After 250k steps, we performed the learning rate decay. We multiplied $10^{-0.2}$ and $10^{-0.1}$ every 50k step for the analysis-synthesis networks and the others, respectively. We finished the training

if the validation loss converges, which took no more than 500k steps for the analysis-synthesis and 1M steps for the others.

C. Evaluation Metrics

We evaluated our networks with the match loss $\mathcal{L}_{\text{MATCH}}$ and reverberation parameter differences (RPDs), i.e., reverberation time T₃₀, direct-to-reverberant ratio DRR, and clarity C₅₀ difference [60], [61]. We report both full-band RPDs (FULL) and average RPDs measured at octave bands of center frequencies 125, 250, 500, 1k, 2k, 4k and 8kHz (FREQ). Since our models generate an IR of 2.5 seconds, we cropped the ground truth if it is longer than that and then calculated the RPDs.

We can interpret the calculated RPDs by comparing them with their respective Just Noticeable Differences (JNDs) [9]. Reported JNDs of T₃₀ from previous works vary from 5% [62] up to about 25% [63]. For C₅₀, 1dB [64] and 1.1dB [65] were reported. DRR's JND differs for various range, e.g., 6dB at -10dB , 2dB at 0dB , 3dB at 10dB , and 8dB at 20dB [66].

D. Subjective Listening Test

Similar to the previous reverb-matching research [10], we conducted a modified version of the MUSHRA test [67]. We asked subjects to evaluate similarities of reverberation between a given reference reverberant speech $h * x$ and followings (h and x denote a test RIR and dry speech signal, respectively).

- A hidden reference $h * x$ (exactly the same audio).
- A lower anchor $h' * x$ obtained by sampling another RIR.
- Estimations to evaluate $\hat{H}_1(x), \dots, \hat{H}_n(x)$. We used the AR models $\hat{H}_1, \dots, \hat{H}_n$ to obtain the reverberant speech.

We crowd-sourced the evaluation with Amazon Mechanical Turk. A total of 60 tasks were evaluated, and at least 5 subjects scored each task. We post-screened the responses whose hidden reference score was lower than the third quartile of their scores.

E. Baselines

We compared our framework with following baselines. Refer to Appendix B for further implementation details.

1) *Parameter-matching Networks*: Similar to the previous non-end-to-end approach [10], we generated the training data with the DAR models and trained the same proposed networks to estimate the original ARPs with a ARP-matching loss. We denote the networks as ASP and BEP for the analysis-synthesis and blind estimation task, respectively.

2) *DNN Decoder*: We trained the same encoder but attached with a decoder, which synthesizes an IR with one-dimensional transposed convolutional layers and TCNs. With this decoder, the entire network resembles an autoencoder. We denote this model as DNN. We trained two DNNs each for the two tasks.

VII. EVALUATION RESULTS

Table I shows the evaluation results. We report average match loss, median RPDs, and average subjective scores (SUBJ) with 95% confidence intervals. We calculated the objective metrics with IRs of the DAR and AR model. In the case of the FDN, we evaluated the AR models in both LTI and LTV versions. These values are written in each cell from left to right (DAR, AR-LTI, AR-LTV). Figure 5 visualizes EDR contours of the ground-truth RIRs, DAR, AR, and the time-varying IR estimated with each network. When the estimation's EDR contours overlay with the ground truth EDR contours, the estimation is accurate.

A. Reliability of the DAR Models

Each DAR model has to be close to its original AR model to make the trained networks reliable. Table I shows that the objective metrics evaluated with the DAR model and the AR model are very close. Due to more time-aliasing and the time variance, the FDN showed more deviation than the other AR models. Nevertheless, the RPD increase or decrease caused by the FSM was much less than the JND value, which indicates that the difference is perceptually unnoticeable. Also, Figure 5 shows that each DAR model's EDR contours are very close to its original AR model's EDR contours. If differences exist, they are mostly in the low-energy regions, which makes them perceptually hard to notice.

B. Comparison with the Baseline Models

1) *Advantage of the End-to-end Learning*: By a large margin, the proposed estimators trained end-to-end outperformed the ARP-matching baselines. While the proposed ones matched the frequency-dependent decay of a target reverberation accurately, the non-end-to-end baselines struggled to do so. A two-sided t-test for each AR model and task showed that the performance difference was statistically significant, with p -values all less than 10^{-5} . This shows that the end-to-end learning enabled by the DAR models gives a huge performance gain.

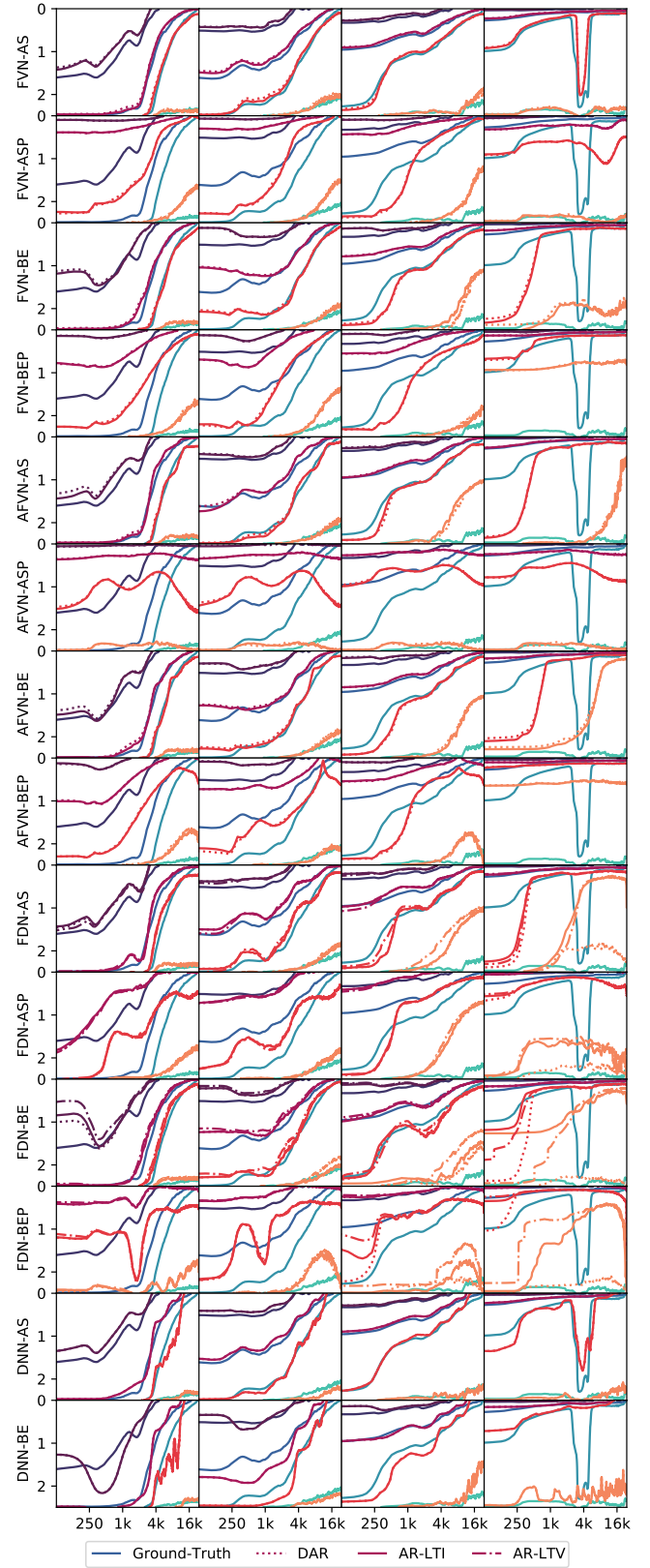


Fig. 5. EDR contour plots of the ground-truth RIRs and their estimations with the trained networks. The x - and y -axis denote frequency (Hz) and time (s). Plots on the same column show the same ground truth (blue curves). Each network's estimations with the DAR, AR models (red curves with different line styles) are drawn for each target. The 0dB, -20dB, -40dB and -60dB contours are drawn, using from the darkest to the brightest colors.

2) *Advantage of the DSP Prior*: Since the DNN baselines have more trainable parameters and complex architecture, they reach lower losses than the DAR-equipped networks. However, they produce audible artifacts. While being more restrictive, the AR models avoid such artifacts and achieve higher subjective listening scores than the DNN baselines. Again, these subjective score differences were statistically significant (all $p < 10^{-5}$). Also, the DNN baselines did not necessarily show superior performance than our methods in terms of the RPD metrics. For example, the analysis-synthesis DNN reported higher RPDs than the proposed FVN analysis-synthesis network except for the frequency-dependent clarity C_{50} difference.

C. Performance Difference Between Target Tasks

Without surprise, the analysis-synthesis networks performed better in most metrics than the blind estimation ones since the target reverberation is directly given, i.e., the analysis-synthesis networks have fewer burdens than the others. Likewise, the both-performing networks show slightly degraded results than their single-task counterparts. Yet, the RPD increases are mostly less than their respective JND values, which hint at a possibility of a universal target-form-agnostic ARP estimation network.

D. AR Model Efficiency and Estimation Performance

Each AR model approximates target reverberation differently, and consequently, its computational efficiency and its estimation networks' performance varies.

1) *Filtered Velvet Noise*: FVN filters each source segment independently (Figure 6 illustrates this). Such flexibility enables its parameter estimators to perform better than the other AR models' counterparts experimented in this paper. However, at the same time, it also has the largest number of ARPs (930), which makes it cumbersome to control manually. Also, it could be computationally expensive to use multiple FVN instances in real-time (2546 FLOPs for each).

2) *Advanced Filtered Velvet Noise*: Instead, AFVN optimizes each coloration filter by decomposing it into the initial coloration and delta-coloration filters, making the model more controllable and efficient (360 ARPs and 1511 FLOPs) than the FVN. Such simplification costs estimation performance since the underlying assumption of the optimization that coloration of real-world RIRs changes gradually does not necessarily hold. In addition, the AFVN networks could be more challenging to optimize than the FVN's since each segment's coloration depends on the previous ones'. Indeed, we empirically observed that their training losses decreased slower than the FVN's.

3) *Feedback Delay Network*: In FDN, we simplified the filter structure even further by using a single absorption filter for each feedback loop. Similar to the AFVN case, FDN trade-offs its estimators' performance with its controllability and efficiency (200 ARPs and 1285 FLOPs). Again, the estimation performance degradation comes from the FDN's restricted expressibility (forced exponential decay) and training difficulty.

VIII. CONCLUSION

In this work, we proposed DAR models that can be integrated with modern DNNs end-to-end. Among many pre-existing AR

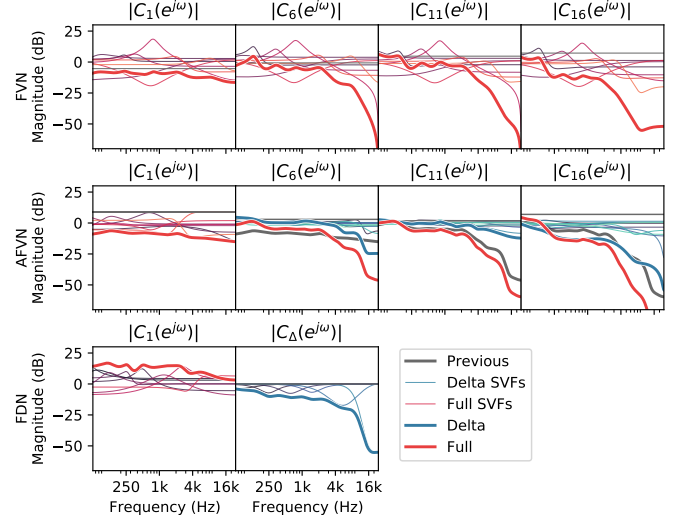


Fig. 6. Magnitude responses of the coloration filters of the AR models. We used the proposed analysis-synthesis networks to obtain the filter parameters for this plot. Each AR model has a different approach to model the frequency-dependent characteristic of given reverberation.

models, we selectively implemented FVN, AFVN, and FDN differentiably. Nonetheless, the suggested method that replaces the IIR parts with FIR approximations using the FSM can be applied to any other AR model. Then, we trained the proposed ARP estimation networks in an end-to-end manner with the DAR models. The evaluation results showed that our networks captured the target reverberation accurately in both analysis-synthesis and blind estimation tasks. Especially, we showed that the end-to-end training improves the estimation performance significantly with a negligible cost of the approximation errors caused by the FSM. Also, we demonstrated that the AR models' structural priors help avoid any perceptual artifact which a DNN as an IR generator could produce. This way, our framework successfully combined powerful and fully general deep-learning methods with well-established DSP knowledge and models for reverberation. In addition, we investigated how each AR model can be compared in terms of its expressive power and parameter optimization difficulty under the deep-learning environment. The evaluation results revealed a trade-off relationship between the estimation performance and compactness of the AR model. Other than the presented AR models and estimation networks, there could be more “deep-learning-friendly” models and “AR-model-friendly” DNNs that yield better performance-efficiency trade-offs, and seeking those is left as future work.

APPENDIX A ABLATIONS AND COMPARISONS OF THE AR/DAR MODELS

A. AR/DAR Model Ablations

We conducted ablation studies to verify that the modifications to the original AR models improve the estimation performance. We evaluated the modified models with the analysis-synthesis task since their performance differences remained the same regardless of the task in our initial experiments.

Table II summarizes the results. FVN, AVFN, and FDN denote the proposed models. $T_i = 10$, $\Delta l_i = L/S$, $-h_0[n]$, and $M = 1$ denote the proposed FVN model without non-uniform pulse distance and allpass filters, non-uniform segmentation, a deterministic FIR, and finer segment gains. Their results show that the proposed modifications contribute to better performance. We omitted the same ablations for the AVFN. Instead, we discarded the initial filter C_1 , delta filter ΔC_j , or both. We also evaluated the FDN without the initial filter C_1 or delta filter C_Δ . The results reveal the importance of modelling the frequency-dependent nature of reverberation.

For FDN, $-\mathbf{Q}_n$, $-\mathbf{U}$, and $-\mathbf{U}, \mathbf{Q}_n$ denote FDN without the time-varying mixing matrix \mathbf{Q}_n , the allpass filters \mathbf{U} , and both, respectively. While $-\mathbf{U}, \mathbf{Q}_n$ reports best evaluation metrics, its low echo density produced unrealistic sound. Using both \mathbf{U} and \mathbf{Q}_n improved plausibility of reverberation with an acceptable performance degradation. Refer to the provided audio samples.

B. Comparisons on Different Coloration Filters

We compared different IIR/FIR filters and parameterization approaches. We evaluated them with the analysis-synthesis task using FVN. Table III summarizes the results. SSVF, PSVF, PEQ, SBIQ, PBIQ, FIR, and LFIR denote serial SVF, parallel SVF, PEQ, serial biquad, parallel biquad, FIR, and linear-phase FIR from [20]. The order of each filter was set to 40. Activation functions and bias initialization for each filter's decoder are as follows. PSVF has the same setting as SSVF. For SBIQ and PBIQ decoders, we used activations from [26], and their biases are initialized to match that of SSVF and PSVF. For PEQ, unlike FDN, we used 10^x for the activation of the gain \mathbf{G} . FIR/LFIR have no activation and custom bias initialization.

In spite of having identical expressive power, SSVF/PSVF performed better than SBIQ/PBIQ by large margins. PEQ performed slightly worse than SSVF due to its restricted degree of freedom. FIR/LFIR also performs worse than SSVF/PSVF and PEQ because they cannot change their frequency responses radically as other IIR filters could.

C. Effects of the Number of Frequency-Sampling Points

Table IV demonstrates the effects of the number of frequency-sampling points N and the regularization loss \mathcal{L}_{REG} . Its notation is similar to Table I, except for the FDN networks whose LTV losses are omitted. Losses of differentiable FDNs with lower N are also omitted since their losses are calculated with shorter IRs. As expected with equation (6), the difference between the DAR loss and true loss decreases with higher N , and use of \mathcal{L}_{REG} ($\beta = 1$) decreased the difference. Moreover, higher N led to better performance, which might be because increased resolution helped each network to find better ARPs.

APPENDIX B DETAILS ON THE BASELINE METHODS

A. ARP Match Models

1) *Training*: We trained the ARP match baseline models as follows. First, we randomized ARPs $\mathbf{P}_1, \dots, \mathbf{P}_n$ and generated an IR with using the DAR model. Then, each baseline network

TABLE II
ABLATION ON THE AR/DAR MODEL CONFIGURATIONS.

MODEL	$\mathcal{L}_{\text{MATCH}} \times 10^{-1}$	T ₃₀ (%)		DRR (dB)		C ₅₀ (dB)	
		FULL	FREQ	FULL	FREQ	FULL	FREQ
FVN	1.236	1.89	4.20	0.94	3.39	0.60	1.95
$T_i = 10$	1.257	2.74	6.14	1.56	4.21	0.48	2.25
$\Delta l_i = L/S$	1.255	2.56	5.43	1.48	3.68	0.89	2.29
$-h_0[n]$	1.250	2.23	10.71	3.17	11.94	0.81	9.88
$M = 1$	1.261	2.53	4.42	1.51	3.65	0.82	2.21
AVFN	1.277	4.77	9.96	1.59	3.64	0.61	2.06
$-C_1$	1.446	6.75	12.60	1.46	8.43	1.76	3.64
$-\Delta C_j$	1.324	7.12	32.16	2.99	5.01	0.92	2.62
$-C_1, \Delta C_j$	1.695	8.91	28.21	2.15	6.62	2.64	5.89
FDN	1.334	8.47	11.59	1.71	3.83	1.08	2.30
$-C_1$	1.446	10.47	20.75	3.69	4.55	2.31	3.03
$-C_\Delta$	1.351	7.83	31.22	2.22	4.71	0.94	2.38
$-C_1, C_\Delta$	1.729	11.62	31.20	4.00	6.68	2.03	4.54
$-\mathbf{Q}_n$	1.307	5.93	12.48	1.81	3.93	1.08	2.39
$-\mathbf{U}$	1.535	21.10	10.76	1.03	3.44	0.88	2.28
$-\mathbf{U}, \mathbf{Q}_n$	1.251	7.43	10.79	1.00	3.39	0.70	2.09

TABLE III
ANALYSIS-SYNTHESIS TASK RESULTS OF DIFFERENTIABLE FVN WITH VARIOUS COLORATION FILTERS AND PARAMETERIZATION APPROACHES.

FILTER	$\mathcal{L}_{\text{MATCH}} \times 10^{-1}$	T ₃₀ (%)		DRR (dB)		C ₅₀ (dB)	
		FULL	FREQ	FULL	FREQ	FULL	FREQ
SSVF	1.236	1.89	4.20	0.94	3.39	0.60	1.95
PSVF	1.235	1.95	4.52	0.96	3.64	0.53	1.86
PEQ	1.254	2.50	5.47	0.97	3.61	0.62	1.89
SBIQ	1.322	3.83	9.44	1.55	4.61	0.59	2.38
PBIQ	1.337	4.88	11.77	1.57	4.01	0.62	2.19
FIR	1.370	2.72	10.10	1.80	3.73	0.51	2.16
LFIR	1.384	3.54	11.84	1.64	4.31	0.62	2.65

estimated ARPs $\hat{\mathbf{P}}_1, \dots, \hat{\mathbf{P}}_n$ from the given IR. We evaluated the estimation and trained the baseline using an ARP-match loss \mathcal{L}_{ARP} defined as follows,

$$\mathcal{L}_{\text{ARP}}(\mathbf{P}_i, \hat{\mathbf{P}}_i) = \sum_i \alpha_i \left\| f_i(\mathbf{P}_i) - f_i(\hat{\mathbf{P}}_i) \right\|_1. \quad (24)$$

Here, the index i denotes a different ARP tensor, e.g., $\mathbf{P}_0 = \mathbf{g}$ and $\mathbf{P}_1 = \mathbf{h}_0$. $f_i(\cdot)$ and α_i are an elementwise function and a constant, respectively. For all DAR models, we set the constant to $\alpha_i = 10$ for the bypass FIRs. We also used $\alpha_i = 10$ for the FDN's absorption filter parameters. We used $f_i(x) = \log_{10}(x)$ for the segment gains of FVN and AVFN. We chose $f_i(x) = x$ and $\alpha_i = 1$ otherwise.

2) *Network Architecture*: We trained an almost identical network to the proposed network for each model/task. The only difference is that we added an activation $10^{-\zeta(x)/20}$ to the \mathbf{g} decoders of FVN and AVFN to improve their performance.

3) *Data Generation*: We tuned each DAR model's ARP randomization scheme to match the synthesized IRs' reverberation parameter statistics to the validation set. For the FVN baselines, we first sampled a reverberation time $T_{30} \sim \mathcal{U}_{\log}[50\text{ms}, 8\text{s}]$ then generated the segment gains \mathbf{g} that match the T_{30} . Here, $\mathcal{U}_{\log}[\cdot, \cdot)$ denotes a uniform distribution in log scale. In this procedure, we also compensated the average pulse distance by

TABLE IV
MATCH LOSS $\mathcal{L}_{\text{MATCH}}$ DIFFERENCE DUE TO THE NUMBER OF FREQUENCY-SAMPLING POINT N AND REGULARIZATION.

MODEL	FREQUENCY-SAMPLING POINTS N			
	$\times 1$	$\times 0.5$	$\times 0.25$	$\times 0.125$
FVN $_{\beta=1}$	1.236	1.236	1.259	1.259
FVN $_{\beta=0}$	1.231	1.237	1.283	1.282
FDN	1.277	1.307	1.328	1.361
				1.393

dividing each gain g_i by $\sqrt{T_i}$. For the initial coloration filter C_1 , we first generated PEQ parameters as $\omega_i \sim \mathcal{U}_{\log}[40\text{Hz}, 16\text{kHz}]$, $R_i \sim \mathcal{U}_{\log}[0.2, 5]$, and $G_i \sim \mathcal{U}[-18\text{dB}, 18\text{dB}]$ (we sorted the cutoff frequencies after the sampling) and derived their SVF parameters. After that, we perturbed each parameter's value slightly. This ARP generation method was motivated by the observation that the differentiable SVFs act like a relaxed PEQ (see Figure 3c). We gradually changed the parameters of C_1 to obtain C_2, \dots, C_K , modeling the frequency-dependent decay. Finally, we set $h_0[n]$ as a short burst of uniform noise with a gain sampled from $\mathcal{U}[-24\text{dB}, 0\text{dB}]$. We followed similar procedures to generate training data for the AFVN baselines. One difference is that the first delta filter $C_{\Delta 2}$ is randomized and the delta filters afterwards are slight deviation of the first one. For the FDN baselines, we sampled each PEQ absorption filter's gain with $G_i \sim \mathcal{U}[-2.8\text{dB}, 0\text{dB}]$.

B. DNN Decoder Models

Regarding the first and second axis of the shared latent \mathbf{z} as a time and channel axis, respectively, our decoder upsamples \mathbf{z} with seven one-dimensional transposed convolution layers. Configurations of these layers are as follows. Channels: 128, 128, 64, 64, 64, 64, then 64. Kernel sizes: 5, 5, 5, 5, 5, 5, then 3. Strides: 3, 3, 3, 3, 3, 3, then 2. Furthermore, we inserted a small TCN after each of the transposed convolutions. The TCNs' configurations are as follows. Channels: 128, 128, 64, 64, 64, 64, and 64. The number of layers: 3, 3, 2, 2, 2, 2, and 2. Kernel sizes: all 7. Finally, we added 1×1 convolution as the last layer to mix all channels. We used the ReLU activation between the layers. This decoder has about 2.5M parameters.

APPENDIX C

DETAILS ON THE FREQUENCY-SAMPLING METHOD

A. Proof of Equation 6

With equation (5), the time-aliasing error can be written as

$$\|H - H_N\|_2^2 = \sum_{n=0}^{N-1} \left| \sum_{m=1}^{\infty} h[mN+n] \right|^2 + \sum_{n=N}^{\infty} |h[n]|^2. \quad (25)$$

With the triangle inequality and $\|X\|_2^2 \leq \|X\|_1^2$, we can upper-bound $\|H - H_N\|_2^2$ with $2S_N^2$ where $S_N = \sum_{n=N}^{\infty} |h[n]|$ is an absolute sum of the tail of the original IR $h[n]$ ($n \geq N$).

Next, we expand $h[n]$ with *partial fraction expansion* (PFE) [68], [69]. For $H(z)$ with M distinct poles where each of them $\nu_i \in \mathbb{C}$ has multiplicity $r_i \in \mathbb{N}$, we can express $h[n]$ as a sum of an FIR $h^{\text{FIR}}[n]$ and IIRs $h_{i,k}^{\text{PFE}}[n]$ where following holds,

$$H(z) = H^{\text{FIR}}(z) + \sum_{i=1}^M \sum_{k=1}^{r_i} \frac{\zeta_{i,k}}{(1 - \nu_i z^{-1})^k}. \quad (\zeta_{i,k} \in \mathbb{C}) \quad (26)$$

Then, applying the triangle inequality to the PFE summation gives an upper bound U_N , an absolute sum of the PFE terms' tails as follows,

$$S_N \leq \sum_{i=1}^M \sum_{k=1}^{r_i} \sum_{n=N}^{\infty} |h_{i,k}^{\text{PFE}}[n]| = U_N. \quad (27)$$

From above equation, each PFE term, first sum, and second sum show $O(n^{k-1}|\nu_i|^n)$, $O(N^{k-1}|\nu_i|^N)$, and $O(N^{r_i-1}|\nu_i|^N)$ asymptotic behavior, respectively [69]. We conclude the proof:

$$\|H - H_N\|_2 \leq \sqrt{2}S_N \leq \sqrt{2}U_N = \sum_{i=1}^M O(N^{r_i-1}|\nu_i|^N). \quad (28)$$

B. Proof of Equation 8

We denote $H(e^{j\omega})$ and $\partial X / \partial p$ with H and X' . X'_N denotes $(X_N)' = (X')_N$. We upper-bound the gradient difference $\Delta \mathcal{G}$ using integral inequalities as

$$\Delta \mathcal{G} \leq \underbrace{\int_0^{2\pi} |H_t(H' - H'_N)| \frac{d\omega}{\pi}}_{\leq 2\|H_t\|_2\|H - H'_N\|_2} + \underbrace{\int_0^{2\pi} |HH' - H_N H'_N| \frac{d\omega}{\pi}}_{\leq 2\|HH' - H_N H'_N\|_2} \quad (29)$$

where the under-braced ones are the Cauchy-Schwartz inequalities. Considering the first integral's upper bound, $\|H_t\|_2$ is a finite constant. In $\|H' - H'_N\|_2$, H' is another stable LTI filter if p is well-defined. If ν_i is a function of p , its multiplicity r_i is doubled in H' . In the worst case, p controls every pole of H and $\|H' - H'_N\|_2 = \sum_{i=1}^M O(N^{2r_i-1}|\nu_i|^N)$ holds. Similarly, the upper bound of the second integral consists an l_2 distance between HH' and $H_N H'_N$. Since HH' has $2r_i$ or $3r_i$ multiplicity for each pole ν_i , $\|HH' - H_N H'_N\|_2 = \sum_{i=1}^M O(N^{3r_i-1}|\nu_i|^N)$ holds at the worst case, which concludes the proof.

REFERENCES

- [1] J. W. Bayless, "Innovations in studio design and construction in the capitol tower recording studios," *Journal of the Audio Engineering Society*, vol. 5, no. 2, pp. 71–76, April 1957.
- [2] B. A. Blessler, "An interdisciplinary synthesis of reverberation viewpoints," *Journal of the Audio Engineering Society*, vol. 49, no. 10, pp. 867–903, October 2001.
- [3] J. Traer and J. H. McDermott, "Statistics of natural reverberation enable perceptual separation of sound and space," *Proceedings of the National Academy of Sciences*, vol. 113, no. 48, pp. E7856–E7865, 2016.
- [4] V. Välimäki, J. D. Parker, L. Savioja, J. O. Smith, and J. S. Abel, "Fifty years of artificial reverberation," *IEEE Transactions on Audio, Speech, and Language Processing*, vol. 20, no. 5, pp. 1421–1448, 2012.
- [5] V. Välimäki, J. Parker, L. Savioja, J. O. Smith, and J. Abel, "More than 50 years of artificial reverberation," *Journal of the Audio Engineering Society*, January 2016.
- [6] J. Dattorro, "Effect design, part 1: reverberator and other filters," *Journal of the Audio Engineering Society*, vol. 45, no. 9, pp. 660–684, 1997.
- [7] W. G. Gardner, "A real-time multichannel room simulator," *Journal of the Acoustical Society of America*, vol. 92, pp. 2395–2395, 1992.
- [8] E. De Sena, H. Hacıhabiboglu, Z. Cvetković, and J. O. Smith, "Efficient synthesis of room acoustics via scattering delay networks," *IEEE/ACM Transactions on Audio, Speech, and Language Processing*, vol. 23, no. 9, pp. 1478–1492, 2015.

[9] N. Agus, H. Anderson, J.-M. Chen, S. Lui, and D. Herremans, “Minimally simple binaural room modeling using a single feedback delay network,” *Journal of the Audio Engineering Society*, vol. 66, no. 10, pp. 791–807, October 2018.

[10] A. Sarroff and R. Michaels, “Blind arbitrary reverb matching,” in *Proceedings of the 23rd International Conference on Digital Audio Effects*, 2020.

[11] J.-M. Jot, “An analysis/synthesis approach to real-time artificial reverberation,” in *[Proceedings] ICASSP-92: 1992 IEEE International Conference on Acoustics, Speech, and Signal Processing*, vol. 2, 1992, pp. 221–224.

[12] J. Coggan and W. Pirkle, “Automatic design of feedback delay network reverb parameters for impulse response matching,” *Journal of the Audio Engineering Society*, September 2016.

[13] V. Välimäki, B. Holm-Rasmussen, B. Alary, and H.-M. Lehtonen, “Late reverberation synthesis using filtered velvet noise,” *Applied Sciences*, vol. 7, no. 5, 2017.

[14] N. Peters, J. Choi, and H. Lei, “Matching artificial reverb settings to unknown room recordings: a recommendation system for reverb plugins,” *Journal of the Audio Engineering Society*, October 2012.

[15] J. Shen and R. Duraiswami, “Data-driven feedback delay network construction for real-time virtual room acoustics,” in *Proceedings of the 15th International Conference on Audio Mostly*, ser. AM ’20. New York, NY, USA: Association for Computing Machinery, 2020, p. 46–52.

[16] F. Gao and W. Snelgrove, “An adaptive backpropagation cascade iir filter,” *IEEE Transactions on Circuits and Systems II: Analog and Digital Signal Processing*, vol. 39, no. 9, pp. 606–610, 1992.

[17] A. D. Back and A. C. Tsoi, “Fir and iir synapses, a new neural network architecture for time series modeling,” *Neural Computation*, vol. 3, no. 3, pp. 375–385, 1991.

[18] P. Campolucci, A. Uncini, and F. Piazza, “Fast adaptive iir-mlp neural networks for signal processing applications,” in *1996 IEEE International Conference on Acoustics, Speech, and Signal Processing Conference Proceedings*, vol. 6, 1996, pp. 3529–3532 vol. 6.

[19] J. D. P. Boris Kuznetsov and F. Esqueda, “Differentiable iir filters for machine learning application,” in *Proceedings of the 23rd International Conference on Digital Audio Effects*, 2020.

[20] J. Engel, L. H. Hantrakul, C. Gu, and A. Roberts, “Ddsp: differentiable digital signal processing,” in *International Conference on Learning Representations*, 2020.

[21] M. A. Martinez Ramirez, E. Benetos, and J. D. Reiss, “Modeling plate and spring reverberation using a dsp-informed deep neural network,” *ICASSP 2020 - 2020 IEEE International Conference on Acoustics, Speech and Signal Processing (ICASSP)*, May 2020.

[22] C. J. Steinmetz, J. Pons, S. Pascual, and J. Serrà, “Automatic multitrack mixing with a differentiable mixing console of neural audio effects,” in *ICASSP 2021 - 2021 IEEE International Conference on Acoustics, Speech and Signal Processing (ICASSP)*, 2021, pp. 71–75.

[23] C. J. Steinmetz, V. K. Ithapu, and P. Calamia, “Filtered noise shaping for time domain room impulse response estimation from reverberant speech,” *arXiv preprint arXiv:2107.07503*, 2021.

[24] A. Richard, D. Markovic, I. D. Gebru, S. Krenn, G. A. Butler, F. Torre, and Y. Sheikh, “Neural synthesis of binaural speech,” in *International Conference on Learning Representations*, 2021. [Online]. Available: <https://openreview.net/forum?id=uAX8q61EVRu>

[25] S. Nercessian, “Neural parametric equalizer matching using differentiable biquads,” in *Proceedings of the 23rd International Conference on Digital Audio Effects*, 2020.

[26] S. Nercessian, A. Sarroff, and K. J. Werner, “Lightweight and interpretable neural modeling of an audio distortion effect using hyperconditioned differentiable biquads,” *arXiv preprint arXiv:2103.08709*, 2021.

[27] L. Rabiner, B. Gold, and C. McGonegal, “An approach to the approximation problem for nonrecursive digital filters,” *IEEE Transactions on Audio and Electroacoustics*, vol. 18, no. 2, pp. 83–106, 1970.

[28] J.-M. Jot and A. Chaigne, “Digital delay networks for designing artificial reverberators,” *Journal of the Audio Engineering Society*, February 1991.

[29] S. Bai, J. Z. Kolter, and V. Koltun, “An empirical evaluation of generic convolutional and recurrent networks for sequence modeling,” 2018.

[30] S. Billings and S. Fakhouri, “Identification of systems containing linear dynamic and static nonlinear elements,” *Automatica*, vol. 18, no. 1, pp. 15–26, 1982.

[31] C. J. Steinmetz and J. D. Reiss, “Efficient neural networks for real-time analog audio effect modeling,” *arXiv preprint arXiv:2102.06200*, 2021.

[32] X. Serra and J. Smith, “Spectral modeling synthesis: A sound analysis/synthesis based on a deterministic plus stochastic decomposition,” *Computer Music Journal*, vol. 14, pp. 12–24, 1990.

[33] V. Zavalishin, *The Art of VA Filter Design*. Native Instruments, 2020.

[34] A. Wishnick, “Time-varying filters for musical applications,” in *Proceedings of the 17th International Conference on Digital Audio Effects*, 2014.

[35] R. Ratnam, D. L. Jones, B. C. Wheeler, W. D. O’Brien, C. R. Lansing, and A. S. Feng, “Blind estimation of reverberation time,” *The Journal of the Acoustical Society of America*, vol. 114, no. 5, pp. 2877–2892, 2003.

[36] J. Y. C. Wen, E. A. P. Habets, and P. A. Naylor, “Blind estimation of reverberation time based on the distribution of signal decay rates,” in *2008 IEEE International Conference on Acoustics, Speech and Signal Processing*, 2008, pp. 329–332.

[37] H. Gamper and I. J. Tashev, “Blind reverberation time estimation using a convolutional neural network,” in *2018 16th International Workshop on Acoustic Signal Enhancement (IWAENC)*, 2018, pp. 136–140.

[38] S. Li, R. Schlieper, and J. Peissig, “A hybrid method for blind estimation of frequency dependent reverberation time using speech signals,” in *ICASSP 2019 - 2019 IEEE International Conference on Acoustics, Speech and Signal Processing (ICASSP)*, 2019, pp. 211–215.

[39] S. Schlecht and E. Habets, “Accurate reverberation time control in feedback delay networks,” in *Proceedings of the 20th International Conference on Digital Audio Effects*, September 2017.

[40] K. Prawda, V. Välimäki, and S. Schlecht, “Improved reverberation time control for feedback delay networks,” in *Proceedings of the 22nd International Conference on Digital Audio Effects*, September 2019.

[41] E. T. Chourdakis and J. D. Reiss, “A machine-learning approach to application of intelligent artificial reverberation,” *Journal of the Audio Engineering Society*, vol. 65, no. 1/2, pp. 56–65, January 2017.

[42] J. O. Smith, *Mathematics of the Discrete Fourier Transform (DFT)*. <http://www.w3k.org/books/>: W3K Publishing, 2007.

[43] V. Välimäki, H.-M. Lehtonen, and M. Takanen, “A perceptual study on velvet noise and its variants at different pulse densities,” *IEEE Transactions on Audio, Speech, and Language Processing*, vol. 21, no. 7, pp. 1481–1488, 2013.

[44] H. Järveläinen and M. Karjalainen, “Reverberation modeling using velvet noise,” *Journal of the audio engineering society*, March 2007.

[45] M. R. Schroeder and B. F. Logan, “‘colorless’ artificial reverberation,” *Journal of the Audio Engineering Society*, vol. 9, no. 3, pp. 192–197, July 1961.

[46] S. Schlecht, “Fdntb: The feedback delay network toolbox,” in *Proceedings of the 23rd International Conference on Digital Audio Effects*, 2020.

[47] S. J. Schlecht and E. A. P. Habets, “Time-varying feedback matrices in feedback delay networks and their application in artificial reverberation,” *The Journal of the Acoustical Society of America*, vol. 138, no. 3, pp. 1389–1398, 2015.

[48] D. Rocchesso and J. O. Smith, “Circulant and elliptic feedback delay networks for artificial reverberation,” *IEEE Transactions on Speech and Audio Processing*, vol. 5, no. 1, pp. 51–63, 1997.

[49] R. Väänänen, V. Välimäki, J. Huopaniemi, and M. Karjalainen, “Efficient and parametric reverberator for room acoustics modeling,” 09 1997.

[50] J. Chung, C. Gulcehre, K. Cho, and Y. Bengio, “Empirical evaluation of gated recurrent neural networks on sequence modeling,” *arXiv preprint arXiv:1412.3555*, 2014.

[51] J. L. Ba, J. R. Kiros, and G. E. Hinton, “Layer normalization,” *arXiv preprint arXiv:1607.06450*, 2016.

[52] S. Shelley and D. Murphy, “Openair: An interactive auralization web resource and database,” *129th Audio Engineering Society Convention 2010*, vol. 2, pp. 1270–1278, 01 2010.

[53] J. Eaton, N. D. Gaubitch, A. H. Moore, and P. A. Naylor, “Estimation of room acoustic parameters: The ace challenge,” *IEEE/ACM Transactions on Audio, Speech, and Language Processing*, vol. 24, no. 10, pp. 1681–1693, 2016.

[54] P. Svensson and U. R. Kristiansen, “Computational modelling and simulation of acoustic spaces,” *Journal of the Audio Engineering Society*, June 2002.

[55] R. Scheibler, E. Bezzam, and I. Dokmanic, “Pyroomacoustics: A python package for audio room simulations and array processing algorithms,” *arXiv preprint arXiv:1710.04196*, 2017.

[56] G. Defrance, L. Daudet, and J.-D. Polack, “Finding the onset of a room impulse response: straightforward?” *The Journal of the Acoustical Society of America*, vol. 124, no. 4, pp. EL248–EL254, 2008.

[57] N. J. Bryan, “Impulse response data augmentation and deep neural networks for blind room acoustic parameter estimation,” in *ICASSP 2020 - 2020 IEEE International Conference on Acoustics, Speech and Signal Processing (ICASSP)*, 2020, pp. 1–5.

[58] J. Yamagishi, C. Veaux, K. MacDonald *et al.*, “Cstr vctk corpus: English multi-speaker corpus for cstr voice cloning toolkit (version 0.92),” 2019.

[59] D. P. Kingma and J. Ba, “Adam: A method for stochastic optimization,” *arXiv preprint arXiv:1412.6980*, 2017.

- [60] “Acoustics — Measurement of room acoustic parameters — Part 2: Reverberation time in ordinary rooms,” International Organization for Standardization, Geneva, CH, Standard, Mar. 2008.
- [61] C. Hak, R. Wenmaekers, and L. Luxemburg, “Measuring room impulse responses: Impact of the decay range on derived room acoustic parameters,” *Acta Acustica united with Acustica*, vol. 98, 11 2012.
- [62] Z. Meng, F. Zhao, and M. He, “The just noticeable difference of noise length and reverberation perception,” in *2006 International Symposium on Communications and Information Technologies*, 2006, pp. 418–421.
- [63] M. G. Blevins, A. Buck, Z. E. Peng, and L. Wang, “Quantifying the just noticeable difference of reverberation time with band-limited noise centered around 1000 hz using a transformed up-down adaptive method,” June 2013.
- [64] J. Bradley, R. Reich, and S. Norcross, “A just noticeable difference in c50 for speech,” *Applied Acoustics*, vol. 58, no. 2, pp. 99 – 108, 1999.
- [65] F. Martellotta, “The just noticeable difference of center time and clarity index in large reverberant spaces,” *The Journal of the Acoustical Society of America*, vol. 128, pp. 654–63, 08 2010.
- [66] E. Larsen, N. Iyer, C. Lansing, and A. Feng, “On the minimum audible difference in direct-to-reverberant energy ratio,” *The Journal of the Acoustical Society of America*, vol. 124, pp. 450–61, 07 2008.
- [67] “Method for the subjective assessment of intermediate quality level of audio systems,” International Telecommunication Union Radio Communication Assembly, Geneva, CH, Standard, Mar. 2014.
- [68] J. Liski, B. Bank, J. Smith, and V. Välimäki, “Converting series biquad filters into delayed parallel form: Application to graphic equalizers,” *IEEE Transactions on Signal Processing*, vol. PP, pp. 1–1, 05 2019.
- [69] J. O. Smith, *Introduction to Digital Filters with Audio Applications*. W3K Publishing, 2007.